Aeroelastic Uncertainty Quantification Studies Using the S^{4}T Wind Tunnel Model

Melike Nikbay*
National Institute of Aerospace, Hampton, Virginia, 23666, USA
Istanbul Technical University, Maslak, Istanbul, 34469, Turkey
and
Jennifer Heeg †
NASA Langley Research Center, Hampton, Virginia, 23681, USA

This paper originates from the joint efforts of an aeroelastic study team in the Applied Vehicle Technology Panel from NATO Science and Technology Organization, with the Task Group number AVT-191, titled "Application of Sensitivity Analysis and Uncertainty Quantification to Military Vehicle Design." We present aeroelastic uncertainty quantification studies using the SemiSpan Supersonic Transport wind tunnel model at the NASA Langley Research Center. The aeroelastic study team decided treat both structural and aerodynamic input parameters as uncertain and represent them as samples drawn from statistical distributions, propagating them through aeroelastic analysis frameworks. Uncertainty quantification processes require many function evaluations to asses the impact of variations in numerous parameters on the vehicle characteristics, rapidly increasing the computational time requirement relative to that required to assess a system deterministically. The increased computational time is particularly prohibitive if high-fidelity analyses are employed. As a remedy, the Istanbul Technical University team employed an Euler solver in an aeroelastic analysis framework, and implemented reduced order modeling with Polynomial Chaos Expansion and Proper Orthogonal Decomposition to perform the uncertainty propagation. The NASA team chose to reduce the prohibitive computational time by employing linear solution processes. The NASA team also focused on determining input sample distributions.

Nomenclature

LHS	Latin Hypercube Sampling
MCS	Monte Carlo Sampling
PCE	Polynomial Chaos Expansion
POD	Proper Orthogonal Decomposition
ROM	Reduced order model

I. Introduction

Aeroelasticity, as a multidisciplinary research field, investigates the behavior of an elastic structure in the airstream and the interactions between inertial, aerodynamic, and structural forces. With the use of advanced technologies in aircraft design and analysis, the need for predicting such aerostructural interactions by using high-fidelity computational models has increased. Most analysis procedures involving high-fidelity modeling consider the system and solution as deterministic. However, as computational models have advanced, parametric sensitivities have become more intrinsic and more hidden. Recent work has demonstrated solution sensitivity to small changes in geometry, freestream conditions and computational parameter specifications. This sensitivity leads to considering these simulations from an uncertainty standpoint. As another motivation in experiments, input parameters are only controlled to within some precision level and the input and output parameters are only known to within measurement errors. Comparisons between computations and experiments should consider these uncertainties.

*Currently, Senior Research Engineer at National Institute of Aerospace, located at NASA Langley Research Center, Aeronautical Systems Analysis Branch & Associate Professor, Faculty of Aeronautics and Astronautics, AIAA Associate Fellow

†Senior Research Engineer, Aeroelasticity Branch, AIAA Associate Fellow

In the current paper, we endeavor to recast our aeroelastic simulation inputs and outputs to treat the analyses as stochastic processes. Two different approaches and philosophical viewpoints are utilized to quantify the effects of uncertainties in aeroelastic systems. The methods, modeling and results are produced from research efforts of teams from NASA and Istanbul Technical University (ITU). The NASA work utilizes linear aerodynamic modeling, while the ITU work utilizes higher fidelity aerodynamic modeling and a reduced order model (ROM) approach for propagating the uncertain parameters.

A flexible vehicle configuration, the NASA Semispan Supersonic Transport (S^4T) wind tunnel model, was chosen as the basis for uncertainty studies and propagation. The current work utilizes information, analytical models and data reported by the (S^4T) project team in 2012 at a special session at the 53rd AIAA/ASME/ASCE/AHS/ASC Structures, Structural Dynamics and Materials Conference. A program overview paper was authored by Silva[36] that documents the wind tunnel model, four wind tunnel tests conducted between 2007 and 2010, and references laboratory tests and analyses. The products from those efforts are utilized as the starting point for the current uncertainty analyses; these aspects will be further identified in the body of this paper.

The current paper focuses on defining statistical distributions of input parameters, propagating them through the two analysis processes, and examining the statistical distributions of output parameters. The analysis approaches will be described first, followed by a description of the development of an example input parameter distribution to represent uncertainty associated with a structural parameter. Example results from each of the analysis methods will then be presented, followed by discussion and concluding remarks.

II. Analysis Approaches

A. Uncertainty Propagation Using Linear Analyses

The methods, modeling and results generated by the NASA team were produced from linear aerodynamic and structural computations. The models used as the baseline cases came from the project team that designed, tested and analyzed the configuration. The major steps taken in performing the uncertainty propagations were:

- Define input variation
- Generate random input samples
- Generate input file for each input sample
- Perform simulation for each input sample
- Extract output parameters from each simulation
- Perform statistical analyses of the evaluation parameters

Three types of simulations were performed in the NASA analyses: static aeroelastic analyses, normal modes analyses and flutter solutions. Each of the analyses were performed using standard analysis options in MSC NASTRAN.[18] Input and output parameter screening was performed using static aeroelastic analysis. Normal modes analyses were performed to show the sensitivity of modal frequencies to the structural variations. Flutter analyses were performed to show the sensitivity to modal parameters in addition to sensitivity to the more fundamental input parameters.

B. Reduced Order Modeling Using Euler Simulations

The ITU team performed static aeroelastic and flutter analyses of the S^4T wing by using the Polynomial Chaos Expansion (PCE)[22–25] and Proper Orthogonal Decomposition (POD)[27,29–31,33,34] based Reduced Order Models,[26,32] which were generated by using an Euler flow based aeroelastic solver in ZEUS[19] software. The aeroelastic solver of ZEUS employs mode shapes obtained from the NASTRAN modal solver. The ROM results were compared to the initial computational results of the high-fidelity models. These ROMs could predict the responses in a small input data range, and in this case both the PCE and POD methods gave satisfactory results while their accuracies were thoroughly discussed in the present work. Secondly, both the PCE and POD methods were used to construct a ROM, which was accurate when large variations of input parameters were considered. The flutter behavior of the S^4T wing could accurately be predicted over the entire flight regime for Mach numbers ranging from 0.60 to 1.20 by the PCE and POD based ROMs. This will be demonstrated in this paper through detailed comparisons of the flutter results of the ROMs to the initial high-fidelity computational analyses.

Uncertainty distributions of structural and aerodynamic input parameters were then propagated using the ROMs. Output parameters from the reduced order static aeroelastic and flutter analyses were examined to assess the influences

of the input parameters that were varied. The input sampling was performed using Monte Carlo Simulation (MCS) and Latin Hypercube Sampling (LHS) techniques, which are frequently used to propagate uncertainties in a probabilistic framework. The input parameters that were treated as uncertain in these analyses were angle of attack, Young's modulus and dynamic pressure. The influence of the first two were assessed for both the static aeroelastic and flutter analyses. The dynamic pressure uncertainty was only evaluated for the static aeroelastic cases. The output parameters that were examined were flutter frequency, flutter speed, flutter dynamic pressure, lift coefficient (C_L), drag coefficient (C_D), pitching moment coefficient (C_m), and wing tip twist angle.

1. Polynomial Chaos Expansion (PCE) Methodology

Nonintrusive PCE defines a ROM basis in terms of orthogonal polynomials. In the present study, Hermite polynomials are used as the orthogonal polynomials since the input parameters are assumed to vary with respect to Gaussian distribution. The definition of the first few Hermite polynomials are given below in terms of the standard variable, ξ:

$$H_o(\xi) = 1 \tag{1}$$

$$H_1(\xi) = \xi \tag{2}$$

$$H_2(\xi) = \xi^2 - 1 \tag{3}$$

$$H_3(\xi) = \xi^3 - 3\xi \tag{4}$$

$$H_4(\xi) = \xi^4 - 6\xi^2 + 3 \tag{5}$$

$$H_5(\xi) = \xi^5 - 10\xi^3 + 15\xi \tag{6}$$

$$H_6(\xi) = \xi^6 - 15\xi^4 + 45\xi^2 - 15 \tag{7}$$

The chaos coefficients can be calculated by using the following relation for a general physical system:

$$\begin{Bmatrix} u_1 \\ u_2 \\ . \\ . \\ u_n \end{Bmatrix} = \begin{bmatrix} H_{10} & H_{11} & H_{12}. & . & H_{1p} \\ H_{20} & H_{21} & H_{22}. & . & H_{2p} \\ . & . & . & . & . \\ . & . & . & . & . \\ H_{n0} & H_{n1} & H_{n2}. & . & H_{np} \end{bmatrix} \begin{Bmatrix} a_1 \\ a_2 \\ . \\ . \\ a_{p+1} \end{Bmatrix} \tag{8}$$

where u_i ($i = 1$ to n) is an output response that is known from the analyses and a_j ($j = 1$ to $p+1$) shows chaos coefficients to be determined. The order of the approximation is denoted by p and n shows the dimension. In this matrix system, the parameters H_{ij} indicate the multiplication of H_i and H_j functions defined in Eq. (4) to (10). However, in the two-dimensional case, H_j is the function of the first standard random variable, ξ, while H_i is the function of the second standard random variable, η. Since three input parameters are defined in the present work, $H_{ijk} = H_i(\xi) \cdot H_j(\eta) \cdot H_k(\gamma)$ (where γ is also a standard random variable) multiplications should be computed. The ROM can be constructed by using the chaos coefficients. In order to calculate the chaos coefficients, linear regression can be applied. Considering the standard normal variables ξ, η and γ, a general linear regression model, U, can be defined in closed form as below:

$$U = H\hat{a} + \varepsilon \tag{9}$$

where ε denotes the error between real values and approximate values. The regression coefficients, $\hat{a}$, can be computed by using Eq. (10):

$$\hat{a} = (H^T H)^{-1} H^T U \tag{10}$$

After determining the regression coefficients, the ROM to represent the reference initial design can be constructed for the two input variable case by using the relation below:

$$U_j(\xi^*, \eta^*) = a_1 H_{j0}(\xi^*, \eta^*) + a_2 H_{j1}(\xi^*, \eta^*) + ... + a_{p+1} H_{jp}(\xi^*, \eta^*) \tag{11}$$

where ξ^* and η^* are the values of the standard random variables for the case that needs to be computed.

2. *Proper Orthogonal Decomposition (POD) Approach*

The Proper Orthogonal Decomposition (POD) method is used to generate a ROM. The system is defined as a linear combination of independent orthogonal basis functions. The orthogonal functions, called the "POD basis functions," are formulated such that the effect of the first mode is the highest and the second mode is less effective and so on. A physical model with n outputs can be expressed as a linear combination given as below:

$$[y]_{(n\times 1)} = \sum_{j=1}^{k} a_j [\Phi_j]_{(n\times 1)} \tag{12}$$

where y is an output response vector for a snapshot of the input variables, a_j are POD coefficients, Φ_j are POD basis vectors and k is the order of ROM ($k < n$). In this study, the "method of snapshots"[35] is used for creating ROMs. A snapshot matrix T, is an $n \times m$ matrix (m is number of snapshots) and can be constructed by using the output parameters of the system:

$$[T]_{(n\times m)} = \begin{bmatrix} y_1^{(1)} & y_1^{(2)} & . & y_1^{(m)} \\ . & . & . & . \\ . & . & . & . \\ y_n^{(1)} & . & . & y_n^{(m)} \end{bmatrix}_{(n\times m)}$$

Any physical system given with a snapshot matrix can be represented by a surrogate response function which superposes the basic modes of the model. The correlation matrix is defined in terms of the snapshot matrix and the number of POD basis vectors:

$$[C]_{(n\times n)} = \frac{1}{n} [T]_{(n\times m)} \bullet [T]^T_{(m\times n)} \tag{13}$$

The POD basis vectors and coefficients are defined through the eigenvalues and eigenvectors of the correlation matrix $[C]\Phi = \Lambda\Phi$. Singular Value Decomposition (SVD) facilitates the construction of the POD based ROMs. In this method, the factorization of a real matrix, T is given below:

$$[T]_{n\times m} = [U]_{(n\times n)} [\Sigma]_{(n\times m)} [V]^T{}_{(m\times m)} \tag{14}$$

where U, the columns of which consist of the eigenvectors of $[T][T]^T$, is the left singular vector of T and these eigenvectors are POD basis vectors. V, the columns of which consist of the eigenvectors of $[T]^T[T]$, is the right singular vector of T. $[\Sigma]$ is a diagonal matrix representing the square roots of POD eigenvalues, λ_i. The POD coefficients are calculated by projecting the snapshots on the POD basis.

$$a_j = [T_j]^T{}_{(1\times n)} \bullet [\Phi_j]_{(n\times 1)} \tag{15}$$

The number of POD basis vectors is equal to the number of snapshots m (and also POD coefficients), however, the number of retained POD basis vectors (POD modes) k is determined by considering the captured energy from the original model. The total captured energy is defined as:

$$E_{total} = \sum_{i=1}^{k} \lambda_i \tag{16}$$

where λ is the vector of normalized eigenvalues of the correlation matrix, C, and k is the required number of POD modes to reach the specified captured energy level. In the present work, the captured energy level is taken as 99.9 % in all applications.

III. Development of Statistical Distributions of Input Parameters

Development of statistical distributions to represent input parameter variations were performed by the NASA team. The information required to formulate the distributions of structural parameters is discussed in this section. The model hardware, testing and finite element model (FEM) tuning process were the key elements in developing the input parameter distributions. The variations for other input variables that are utilized in the current work—angle of attack, dynamic pressure, Mach number and modal frequencies—are not discussed in detail here; the processes and assumptions for developing these additional input parameter variations are detailed in the NATO-STO-AVT-191 Task Group Report.[17]

A. Hardware Characterization Testing

The S^4T wing is a complex aeroelastic semispan wind tunnel model, which is designed for aeroelastic/ aeroservoelastic analysis.[20] The fuselage consists of a graphite-epoxy flexible beam attached to an aluminum C-channel rigid beam. Wingbox construction consists of an upper and lower skin, each made from fiberglass/epoxy face sheets sandwiching a paper honeycomb core. Figure 1 shows the configuration.

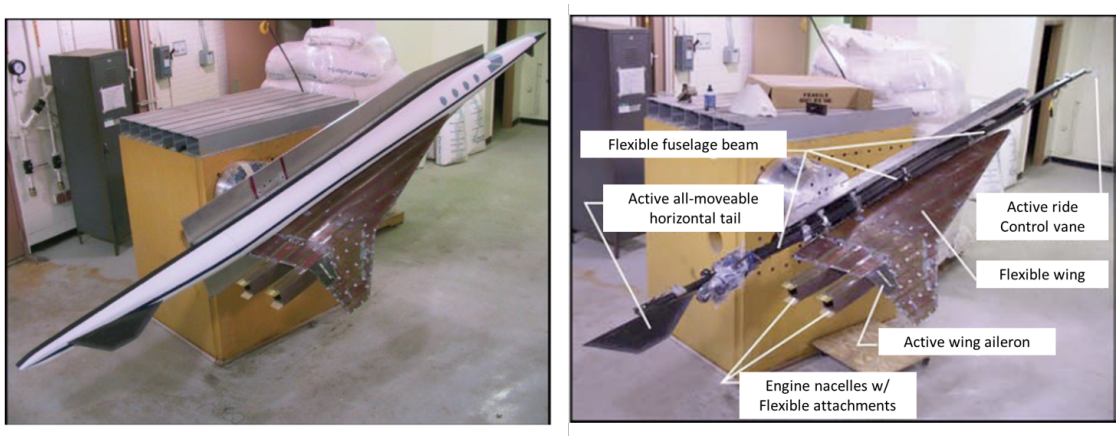

Figure 1. S^4T configuration.

Extensive wing geometry measurement, stiffness testing and modal survey testing (ground vibration testing, GVT) were performed. These results were used to improve the aerodynamic surface definition and the structural model. The flexible fuselage beam element material properties were used as principal tuning parameters during model update procedures. Figure 2 shows the results from tuning the analytical model to match the measured deflections. The range of the modifications used in performing this tuning serve as the basis for the material property distributions used in the uncertainty propagation studies.

The GVT results[37]contain measured values for the frequencies and damping values associated with the first six modes. The analytical and measured frequencies and descriptions of the mode shapes are shown in Table 1.[38] Comparisons of the analytical and measured frequencies give indications of the success level of the stiffness tuning exercise. The scatter among the measured values for each modal frequency also provides an indication of the variation associated with measuring the frequencies. Measured damping values, reported in reference 37, contained significant scatter.

B. Structural Model

The FEM utilized in this study for the baseline analysis cases is the unmodified model from the S^4T team that is detailed by Sanetrik.[38] The FEM elements, emphasizing the fuselage, are shown in Figures 3, 4 and 5. Figure 5 in particular shows the flexible fuselage beam material property segments that will be modified as part of the uncertainty propagation studies. The numbers given in the figure correspond to the designations used for material property characterization sets. Associated with each material property set is a value for density, Young's modulus, the shear modulus and Poisson ratio. In the current studies, the only material property to be treated as an uncertain variable is the Young's modulus.

The fuselage beam elements shown in Figure 5 were considered the primary candidates for parametric variation in this study, based on the tuning processes of the S^4T team. The input variable ranges were based on the values used by

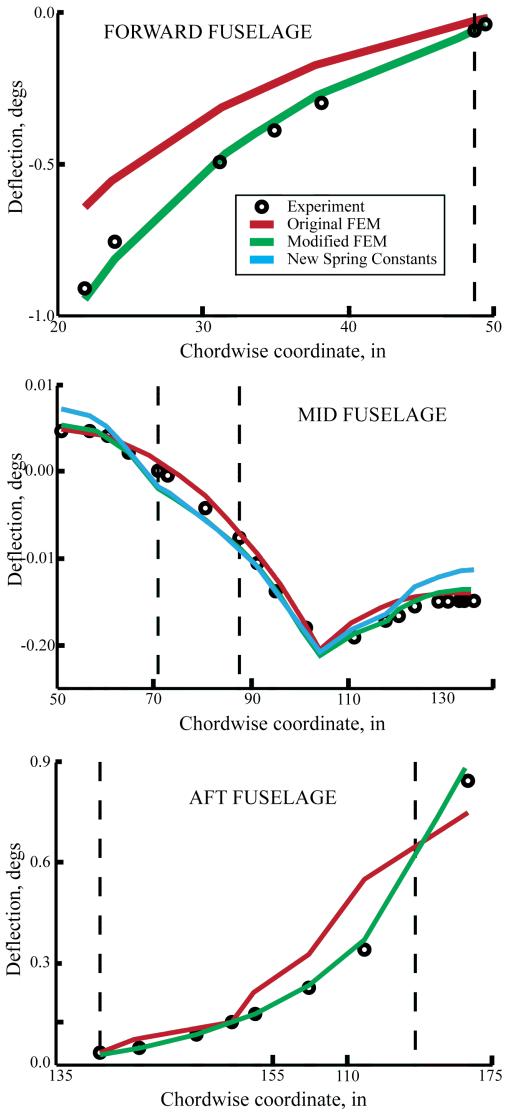

Figure 2. Finite element model tuning by S^{4}T test team; Deflection in degrees vs Flow-wise (chordwise) station.

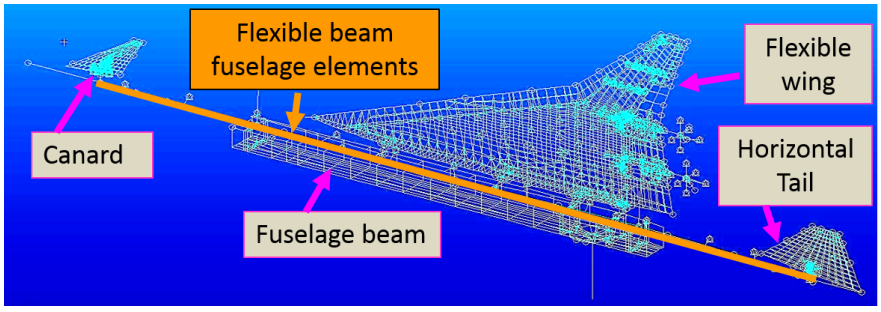

Figure 3. Finite element structural model.

the S^{4}T test team to tune the FEM. During this procedure, the S^{4}T team tuned the six beam materials in the baseline structural model, correlating with measured deflection data, as shown in Figure 2. In the current study, these same six material properties were evaluated, using minimum, nominal and maximum values employed in the original tuning

Table 1. Measured and analytical modal frequencies, Hz.

		Modal frequencies, Hz			
Mode	**Description**	**Analytical nominal value**	Measured values		
1	**Pitch about forward nodal mount**	6.29	6.395	6.375	6.249
2	**Pitch about balance**	8.43	8.089	7.935	7.838
3	**Fuselage 1st bending**	10.07	10.323	10.312	10.059
4	**Wing 1st bending**	11.4	11.635	-	11.781
5	-	12.88	12.528	12.585	12.384
6	-	14.25	16.571	15.066	15.603
7	-	15.28	-	-	-
8	-	17.6	-	-	-

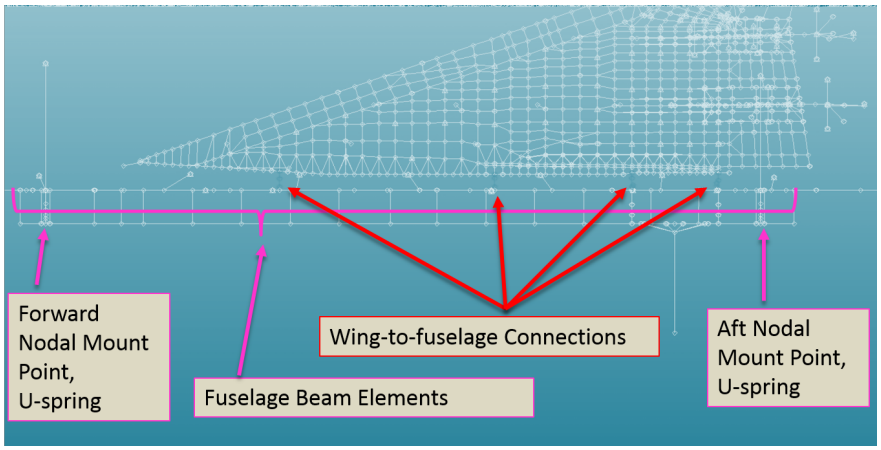

Figure 4. Finite element model: Connection points from fuselage to wing, nodal mount points and fuselage beam elements.

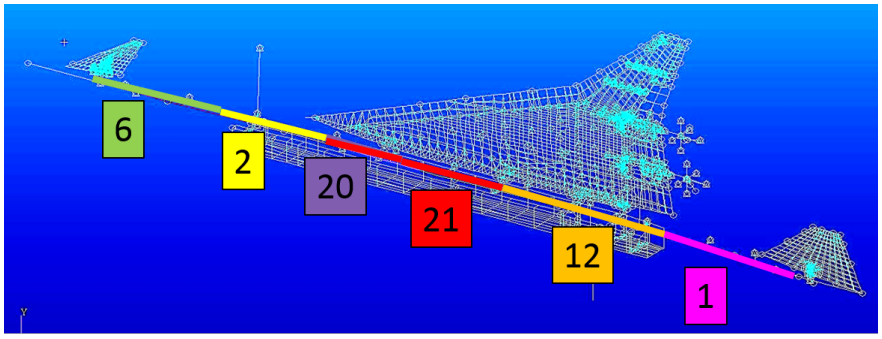

Figure 5. Beam elements' material property numbers.

process. The values chosen by the S4T team to use in the final version of the FEM were designated as the nominal values.

Three input distributions and drawn sample sets characterizing the uncertainty of the Young's modulus were generated: 1) a normal distribution sampled with LHS, 500 samples drawn without replacement; 2) a normal distribution sampled with LHS, 25 regions with 25 resamplings with replacement (625 total samples); and 3) a uniform distribution sampled with LHS, 25 regions with 25 resamplings with replacement (625 total samples). For material 21, which will be shown subsequently to be of greatest interest, the Gaussian distributions from which samples were drawn had a mean value of 6.390e+06 psi and standard deviation of 0.945e+06 psi. The detailed statistics for all three distributions for this material property are given in Table 2.

IV. Linear Analyses

A small subset of the linear analysis results generated in this study are discussed and presented in the current paper. Additional results and comparisons with different uncertainty quantification approaches are detailed in reference 17. In the current section, an example of parameter screening using static aeroelastic analysis is presented, along with an example case of propagating a distribution of an input parameter through a normal modes analysis. Finally, example results are shown for propagating both uniform and normal distributions of an input parameter through the flutter analysis process.

A. Static Aeroelastic Analyses for Parameter Screening

Material property screening studies used the flexible-to-rigid ratio of the lift coefficient due to the horizontal tail deflection as one of the evaluation parameters. This particular output variable was chosen due to several factors: 1) this parameter was shown to be linear with respect to dynamic pressure; 2) the S^{4}T program's main research focus was on aeroservoelasticity, which emphasizes the criticality of control derivatives and 3) most control law designers associated with the program chose the horizontal tail as their actuation surface for performing aeroservoelastic tasks. The screening analysis results, shown in Figure 6, indicate that the Young's modulus associated with the material property 21 has the greatest influence. This is shown by the relative slopes of each of the lines; the slope associated with material property 21 is the steepest.

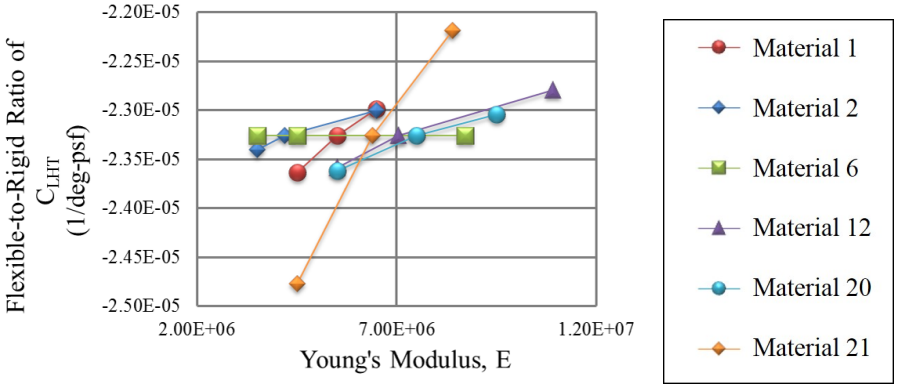

Figure 6. Static aeroelastic analysis parameter screening; Flexible-to-rigid ratio variation of C_{LHT} due to variation of flexible fuselage beam Young's moduli.

Thus, the Young's modulus of material 21 was chosen as the structural model parameter to vary and propagate through static and dynamic aeroelastic simulations. This material property is associated with beam elements comprising the model's fuselage in the region near the mid-chord wing root, as shown in Figure 5.

B. Normal Modes Analysis

The second major type of analysis that was performed using linear methods was normal modes analysis. For this analysis, the input parameter identified as the most significant using the screening analysis was varied—the Young's modulus of material property 21. Any variation in dynamic pressure, Mach number, angle of attack or structural damping would have no impact on the output parameters of a normal modes analysis. The output parameters that are examined here are the frequencies of the first (lowest value) 30 natural modes. The three input distributions shown in Table 2 for the Young's modulus variation were each used as inputs to this process.

Histograms of the first 30 natural frequencies are shown in the 30 subplots of Figure 7 for the second input case as numbered in Table 2. Notice that for the input distribution, which is Gaussian, some of the modal frequency output distributions appear Gaussian and some appear skewed (i.e., some of these output distributions are likely better fit by beta distribution than by Gaussian distributions). There are also a few frequencies where the influence of the input variation is so small that the histogram shows quantization levels associated with the significant digits of the output data file (i.e., the first two subplots in the third row, associated with modes 13 and 14). The results for the second input case are presented in Figure 8. In Figure 8, the mean values for the first 8 modal frequencies are shown by the horizontal lines. The variations in the simulation outputs are captured by the heights of the blue rectangles, indicating

Table 2. Statistical analysis of input distribution samples, Young's modulus varied.

Case	Input distribution type	Sampling Method	Mean	Standard deviation	Skewness	Kurtosis	Coefficient of variation
1	Gaussian	LHS 500 regions, no replacement	6.39E+06	9.45E+05	2.39E-02	2.96E+00	1.48E-01
2	Gaussian	LHS 25 regions 25 resamplings, with replacement	6.39E+06	9.49E+05	-5.91E-02	3.04E+00	1.49E-01
3	Uniform	LHS 25 regions 25 resamplings, with replacement	6.39E+06	1.09E+06	-4.20E-03	-2.90E-01	1.71E-01

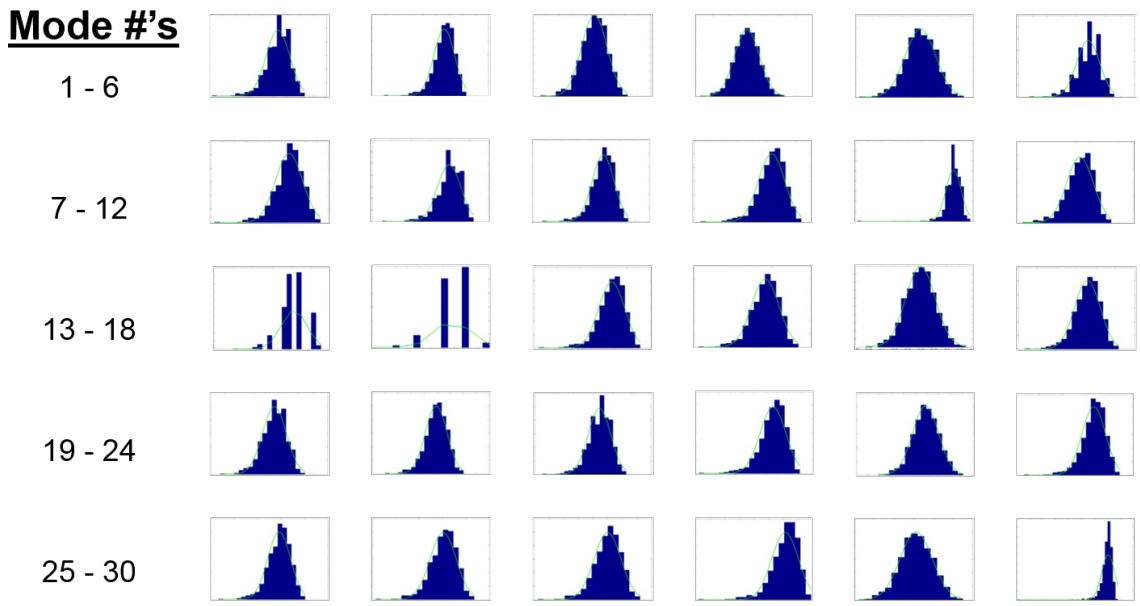

Figure 7. Histograms of the first 30 modal frequencies; Results from LHS (25, 25) samples from Gaussian distribution of the Young's modulus of material 21.

the +/- 3 sigma bounds of the frequencies. The figure shows that only the second and third modes are significantly modified by the variations applied to the Young's modulus.

C. Flutter Analysis

Flutter analyses were conducted for eight baseline cases, and for input parameter variations of each of those eight cases. The baseline cases correspond to the subsonic Mach numbers where the S^4T team generated computational results. Three uncertainty distributions were propagated for each condition for five input parameter sets: structural damping, Young's modulus, Mach number and natural frequencies. Each input distribution was propagated independently. The complete results are given in reference 17. In the current section of this paper, example results are shown for two distributions representing the damping variation. The Gaussian distribution of damping was generated with a mean value of 0.02, and a standard deviation of 0.006; the uniform damping distribution was generated with a minimum value of 0 and a maximum value of 0.04.

The doublet lattice method was employed to generate the aerodynamics and the PKNL (p-k nonlinear) flutter solution of MSC/NASTRAN was employed. For each of these baseline cases, the structural damping was set to zero, and the first thirty flexible modes were included in the structural definition, corresponding to including all modes

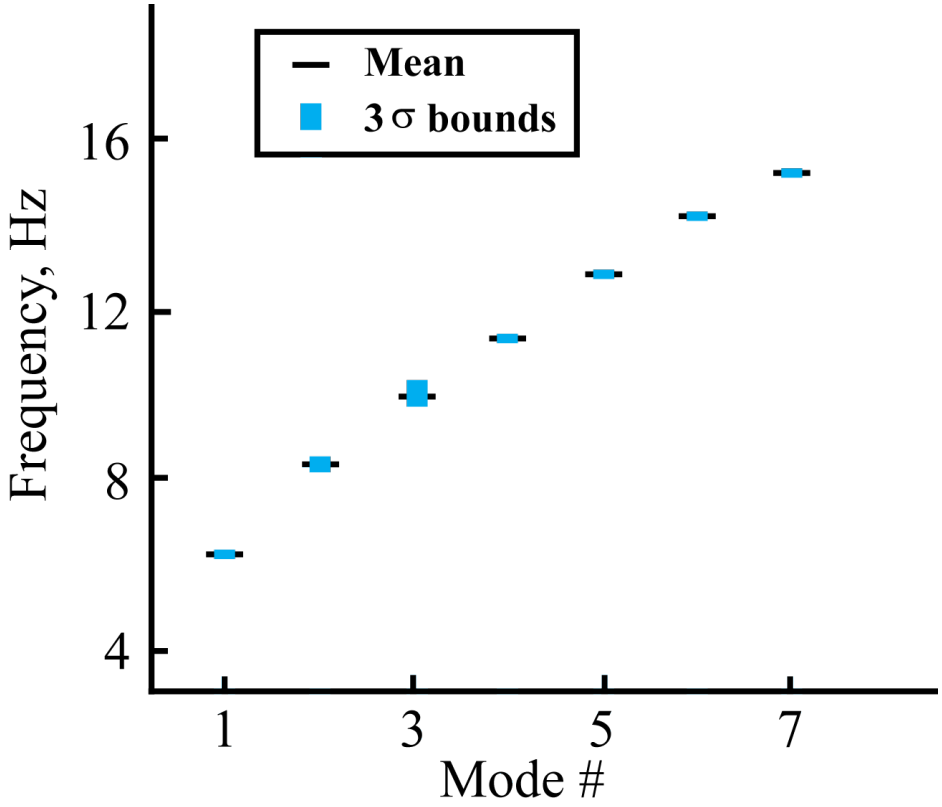

Figure 8. Variation of Young's modulus for material 21, Gaussian LHS (25, 25); Influence on the first 8 modal frequencies.

below 100 Hz. The flutter analyses were performed echoing the baseline process performed by the S^4T team, keeping the velocity constant and varying the density. Although flutter results are shown here at transonic Mach numbers (Mach 0.80 and 0.95), this should not be interpreted as an endorsement to utilize linear methods in this range. The results are possibly relevant at Mach 0.8 for low angles of attack, but this must be established by comparisons with the experimental data or higher fidelity simulations.

In linear analysis, the flutter condition is defined as the dynamic pressure that causes a mode to have a damping value of zero. The structural damping appears in the flutter solution equations as an additive term. Once the aeroelastic modal damping has been calculated, changes due to the structural damping can be approximated by using the structural damping as the definition of neutral stability, rather than using the value of 0. This is not an exact calculation due to the presence of nonlinearities introduced by the generalized aerodynamic forces, which are calculated as functions of reduced frequency and thus are functions of structural damping. These influences are small and are neglected here.

The derivative of the aeroelastic damping with respect to dynamic pressure is referred to as the steepness of the flutter crossing. A steeper flutter crossing corresponds to a case that is more sensitive to aerodynamic damping (or aerodynamic energy input) and less sensitive to structural damping. The higher Mach number cases are more sensitive to aerodynamic loading than those at lower Mach numbers. Conversely, the lower Mach number cases—with flatter flutter crossings—are more sensitive to structural damping than the higher Mach number cases. The result of the difference in the flutter crossing steepness at different Mach numbers is illustrated in Figure 9, where the flutter dynamic pressure variation is observed to be considerably larger at Mach 0.6 than at the higher Mach numbers.

We note that for a Gaussian input distribution of the damping, the output flutter dynamic pressure is also Gaussian. The damping variation flutter results are plotted with the baseline analysis results (shown by the red circles) in Figure 9. In the figure, the output histograms are shown on their sides. The green bar graphs show the histograms of the flutter dynamic pressures due to a uniform input variation of the damping. The height of the histogram (in terms of flutter dynamic pressure) is greatest for the lowest Mach number indicating that the lower Mach number flutter onset is more sensitive to uncertainty in damping than the higher Mach numbers. This reflects the steeper flutter crossing as discussed above. The uniform input distributions result in uniform output distributions. The blue bar graphs shows the histograms of the flutter dynamic pressures due to Gaussian input variation of the damping. In comparing the results

among the Mach numbers, the trend in the range of flutter dynamic pressures are similar to those discussed for the uniform variation. The shapes of the output histograms are Gaussian, reflecting the linear relationship between the flutter dynamic pressure to the damping.

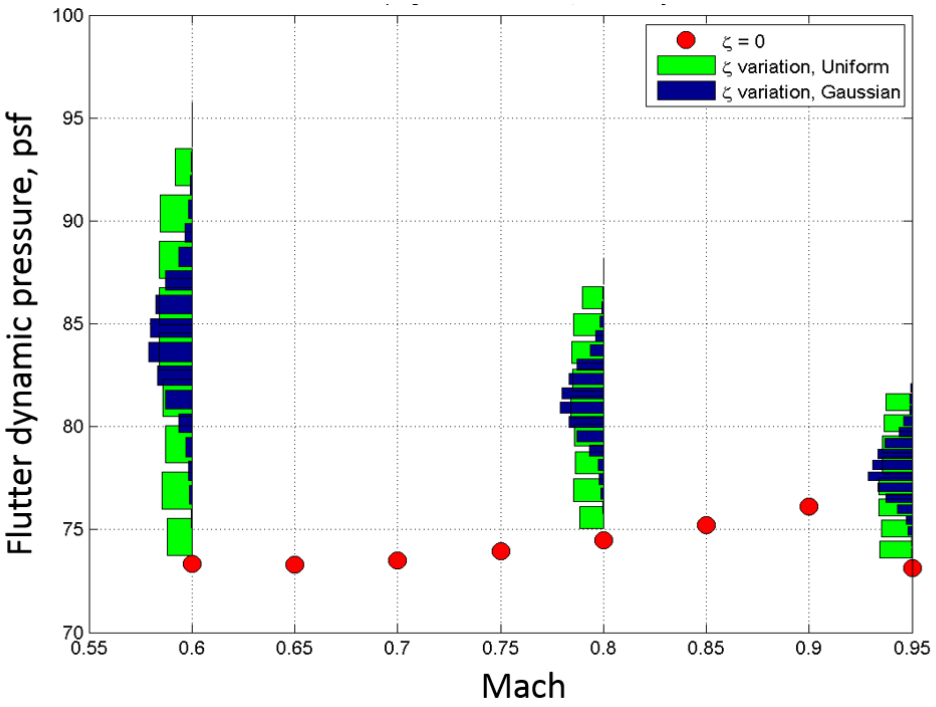

Figure 9. Flutter boundary, including damping variation results.

V. Euler Based Aeroelastic Analysis and Reduced Order Modeling in UQ

In this section, an Euler solver is used to compute the static aeroelastic and flutter responses of the S^4T wing for uncertainty quantification (UQ) process. The Euler solver provides a good balance between the complete modeling of the flow physics and the computational speed needed for repeated function evaluations in UQ. The static aeroelastic and flutter analyses are accomplished for the given reference cases at different flight conditions with various Mach numbers, angles of attack values and dynamic pressures. After performing the sufficient amount of analyses, these high-fidelity computational models are used to produce ROMs. These models enable considerable reduction in computational time while investigating the effects of uncertain input variations on output aeroelastic responses through uncertainty quantification. In the present work, the reduced modeling strategy is used to represent the high-fidelity computational models of the S^4T wing to present accurate solutions while providing a considerable reduction in the computational time.

The fundamental steps of the ROM strategy of this work first require construction and analysis of the high-fidelity computational models. These computational models are developed to perform static aeroelastic and flutter analyses of the S^4T wing in the ZEUS software. ZEUS is an Euler unsteady aerodynamic solver developed for aeroelastic solutions of complex geometries.[19] It involves an automated mesh generation scheme and overset grid capability for complex configurations while using a Cartesian grid and employing boundary layer coupling. It also uses a modal data importer and ZAERO 3D spline module to construct structural grids. ZEUS uses central difference with the JST (Jameson-Schmidt-Turkel) artificial dissipation scheme for flux construction and Green's integral boundary layer method for turbulence model.[21] Aeroelastic analyses in ZEUS require its own input file and a modal solution from a finite element solver. In the present work, Nastran is used as a FEM based structural solver for the modal analysis. An aerodynamic mesh is generated and the fluid structure interaction is provided in ZEUS to perform the required aeroelastic analyses after importing the modal solution. Once the aeroelastic analyses are accomplished for the reference cases, they should be repeated as many times as the design samples generated to construct the ROMs. Different flight conditions

with various Mach numbers, dynamic pressures, and angle of attack values, for a total of 3 reference cases for flutter analyses and 9 reference cases for static aeroelastic analyses are considered. After generating an adequate number of sampling for each reference case, the model reduction is performed by using the nonintrusive Polynomial Chaos Expansion (PCE) and Proper Orthogonal Decomposition (POD) methods. Both the PCE and POD methods aim to ameliorate the computational efficiency.

Firstly, the static aeroelastic and flutter analyses of the S^4T wing were performed for the reference cases by using the PCE and POD based ROMs. Then, the ROM results were compared to the initial computational results of the high-fidelity models. These ROMs could predict the responses in a small input data range, and in this case both the PCE and POD methods give satisfactory results while their accuracies will be thoroughly discussed in the present work.

Secondly, both the PCE and POD methods were used to construct a ROM, which is accurate when large variations of input parameters are considered. The flutter behavior of the S^4T wing could accurately be predicted over the entire flight regime for Mach numbers ranging from 0.60 to 1.20 by the PCE and POD based ROMs. This case will also be evaluated in more detail by comparing the flutter results of the ROMs to the initial high-fidelity computational analyses.

Finally, structural and aerodynamic uncertainties, which influence static aeroelastic and flutter computational solutions, were propagated using ROMs. The uncertainty quantification was performed by using MCS and LHS techniques, which are frequently used to propagate uncertainties in a probabilistic system. The effects of uncertain input variables on the flutter and static aeroelastic responses were investigated. For the static aeroelastic simulations, the uncertain input variables examined were angle of attack, elasticity modulus and dynamic pressure. The static aeroelastic output variables were aerodynamic lift, drag, moment coefficients and wing tip twist angle. For the flutter simulations, the angle of attack and elasticity modulus were the uncertain input variables. The flutter output variables examined were flutter frequency, flutter speed and flutter dynamic pressure.

A. Static Aeroelastic and Flutter Uncertainty Quantification

In the aeroelastic UQ analysis, we used the distributions for the angle of attack and dynamic pressure as given by the AVT-191 task group. Each structural modal solution was used in the aeroelastic analysis and the final results were classified according to the given clusters divided for angle of attack and dynamic pressure values. In our study, instead of giving a distribution to the modal frequencies, elasticity modulus of Material 21 was distributed by using 10 samples with a 5% uncertainty around the mean value of 6.39MPa. However, the uncertainty distributions for the angle of attack and dynamic pressure were the same as provided by the AVT-191 Task Group. These distributions were divided into different clusters and each cluster was defined with a mean value and a standard deviation (see Table 3) with a normal distribution assumption.

Table 3. Clusters for aeroelastic UQ analysis.

Cluster		Angle of attack (degs)		Dynamic pressure (psf)	
Number	Designation	Mean	Standard deviation	Mean	Standard deviation
1	20 psf Cluster 1	0.204571	0.016328	21.40429	0.182254
2	20 psf Cluster 2	0.826455	0.097638	20.17791	0.171811
3	35 psf Cluster	0.327333	0.06912	35.55383	0.397882
4	60 psf Cluster 1	-0.19118	0.065167	60.97871	0.519223
5	60 psf Cluster 2	0.193625	0.043197	60.3455	0.513832

For the static aeroelastic analysis, the proposed UQ procedure is repeated with three Mach numbers set as M=0.60, M=0.85 and M=0.95. The data sampling information in 5 clusters are sequentially run for M=0.60, M=0.85, and M=0.95. In Figure 11 to Figure 13, the random aerodynamic lift coefficient C_L, drag coefficient C_D, moment coefficient C_m and wing tip twist angle values of the S^4T wing are plotted against the angle of attack values for the samples in each cluster.

For the flutter analysis, the proposed UQ procedure is similarly repeated with three Mach numbers set as M=0.60, M=0.85, and M=0.95. The data samples in the 5 clusters used in our dynamic aeroelastic study are sequentially run for M=0.60, M=0.85 and M=0.95. In Figure 14 to Figure 16, the random flutter speed values of the S^4T wing are plotted against the angle of attack values for the samples in each cluster.

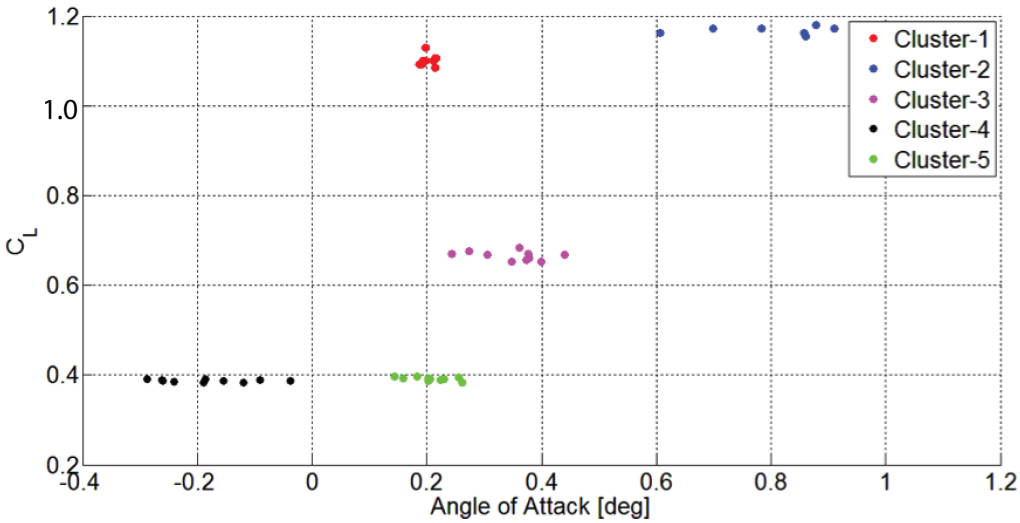

Figure 10. C_L **versus angle of attack for Mach 0.85.**

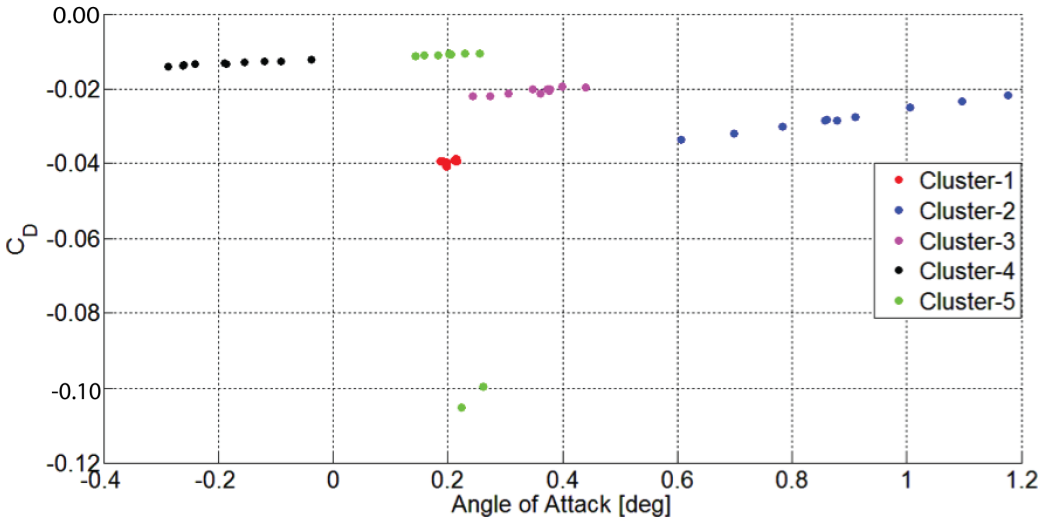

Figure 11. C_D **versus angle of attack for Mach 0.85.**

VI. Discussion

Linear aeroelastic analysis methods result in some input-output relationships that are linear and some that are not. When the relationship is linear, Gaussian input distributions result in Gaussian output distributions. The nonlinear input-output relationships that have been examined here showed that the output data generated due to Gaussian input distributions were characterized by beta distributions. The input-output relationships that are not linear, when subject to a uniform (constant) input, produced triangular output distributions. Regardless of the output distribution shape, maximum likelihood fits to Gaussian distribution parameters were calculated for comparison with other uncertainty propagation analyses performed for this project.

Varying the angle of attack in the linear analysis results in variation only in the trimmed aeroelastic twist angle. The static aeroelastic stability and control derivatives are not functions of the angle of attack, and neither are the flutter results. The twist angle distributions due to Gaussian-distributed angle of attack variations were demonstrated to be directly calculable from the linear relationship properties of the Gaussian statistics.

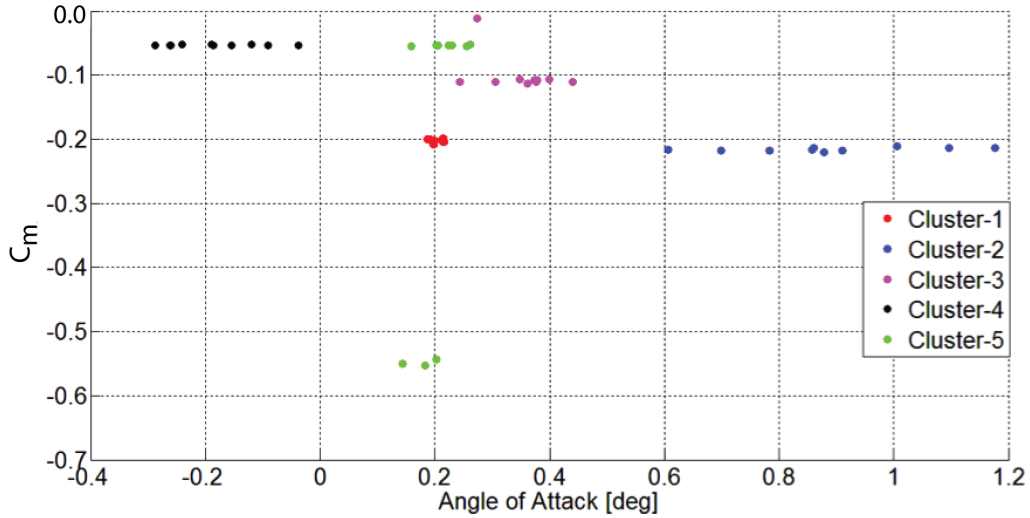

Figure 12. C_m **versus angle of attack for Mach 0.85.**

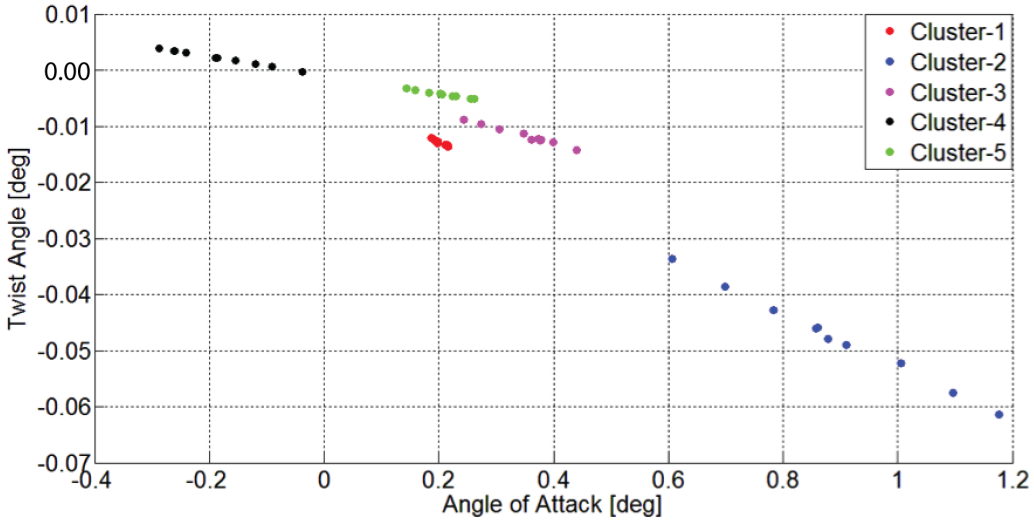

Figure 13. Twist angle versus angle of attack for Mach 0.85.

Modal analysis showed that variations in the natural frequencies due to the variations in Young's modulus were considerably less than the uncertainty levels that are associated with typical structural dynamic representation. That is, the comparison between finite element representation and ground vibration test results is generally greater than the observed output variations produced in this study. This indicates that the frequency variations produced by the current uncertainty propagation will be considerably lower than should be investigated in a flutter uncertainty study. This shortcoming of the current work is expected, as only one region of the FEM was included in the structural property input variations.

On the other hand, the most significant change in the modal frequencies was produced for one of the two modes that was shown to be critical for simulating flutter of this configuration. This indicates that the input parameter screening process, although performed using static aeroelastic analyses, was effective in choosing a parameter that was also significant relative to flutter prediction. In particular, the input parameter screening included evaluating the sensitivity of the lift curve slope, $C_{L\alpha}$ and pitching moment coefficient derivatives due to angle of attack, $C_{m\alpha}$. While these parameters are not direct links to general predictions of flutter, sensitivity of these stability derivatives does

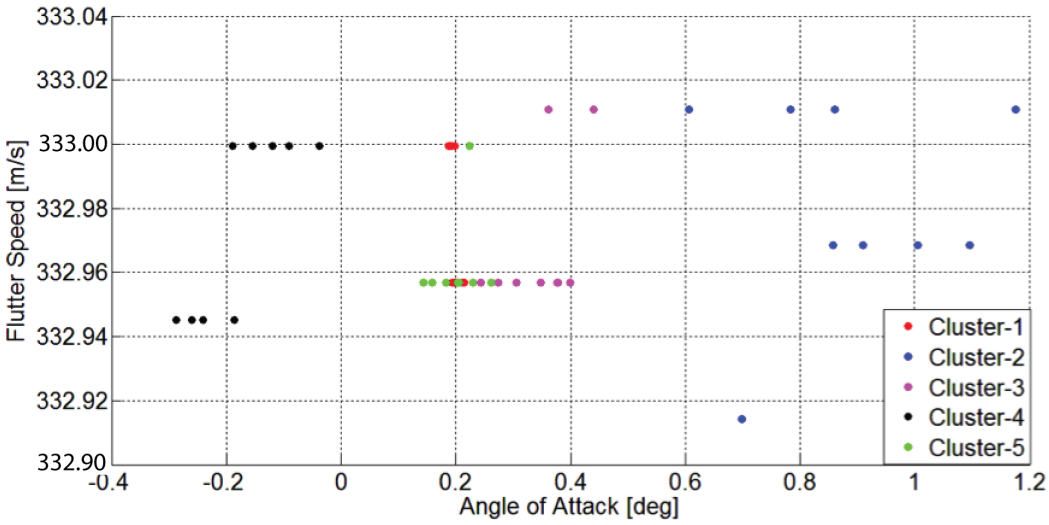

Figure 14. Flutter uncertainty quantification for M=0.60.

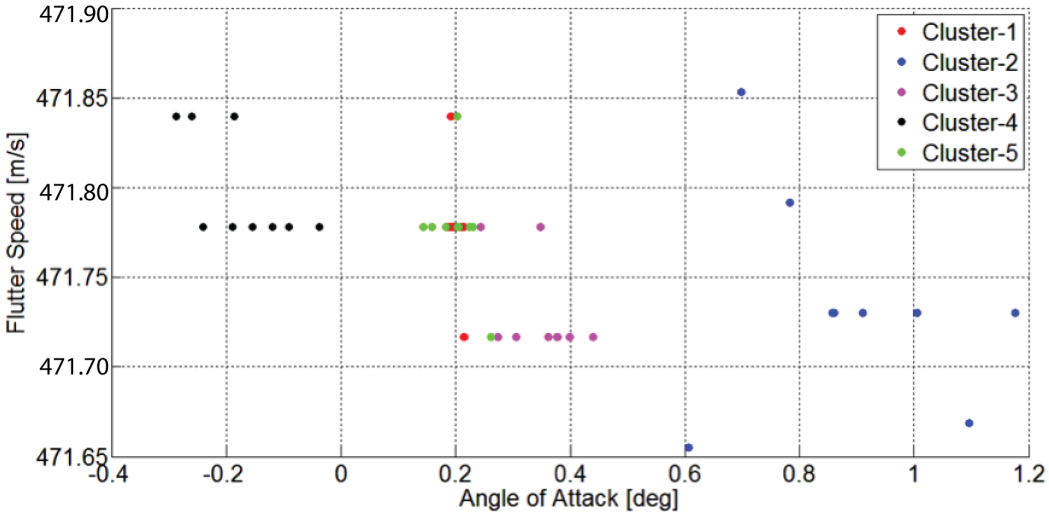

Figure 15. Flutter uncertainty quantification for M=0.85.

provide parameter selection guidance for a configuration where vehicle pitching or wing torsion is involved in the flutter mechanism.

In the second part of the current paper, since the uncertainty quantification using high-fidelity computational models requires a very large amount of computational time, ROMs are generated using a high fidelity aeroelastic framework based on Euler solver and modal aeroelastic coupling. The static aeroelastic and flutter analyses of the S^4T wing are performed by using the generated design samples to construct a ROM. The ROM strategy of the present work is based on PCE and POD techniques. After the construction of the PCE and POD based ROMs, the reference aeroelastic analyses are also performed via these models and their accuracies are evaluated. Finally, the structural and aerodynamic uncertainties are propagated through the reduced models to investigate the randomnesses in the output parameters.

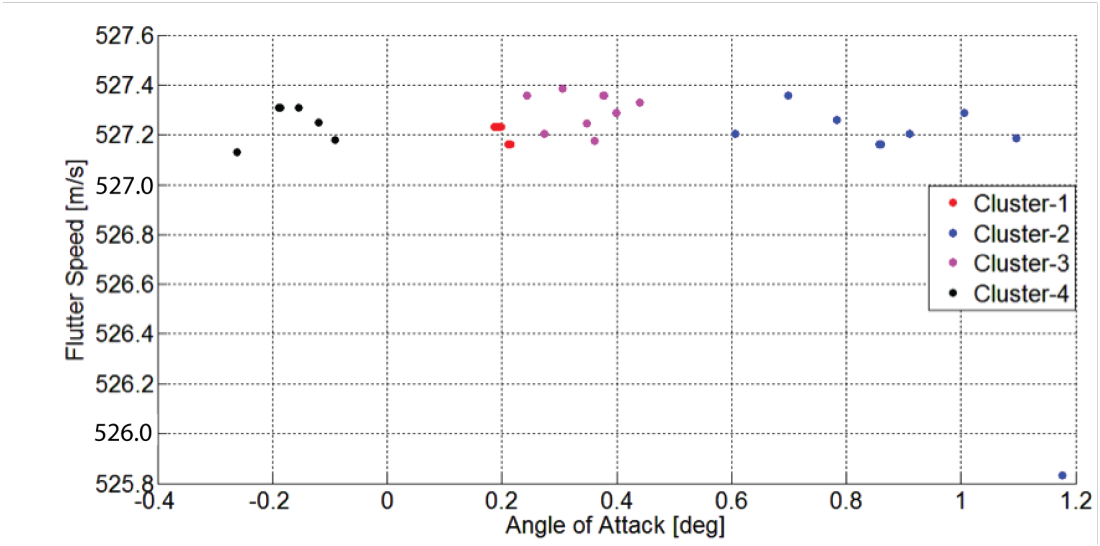

Figure 16. Flutter uncertainty quantification for M=0.95.

VII. Concluding Remarks

The influences of the input distribution type and sampling were examined for several cases. It was demonstrated that where the input-output relationship is approximately linear, an input distribution shape is reproduced in the output distribution shape for both uniform and Gaussian processes. For cases where the relationship is not linear, a Gaussian input distribution can produce output parameters that are skewed and better fit with beta distributions.

Linear analyses are useful for determining which input parameters should have uncertainty distributions assigned. Development of statistical distributions to represent those uncertainties relies heavily on observations made in experimental data sets. Distributions of the input parameters were determined by examining experimental data and by examining the structural model tuning parameters and values that were used by the experiment test team. Parameter screenings using static aeroelastic stability and control coefficients were performed to determine which material property to vary. The flexible-to-rigid ratio of the lift coefficient due to angle of attack and due to the horizontal tail produced the same result: the Young's modulus of the fuselage elements at the wing centerline had the greatest influence on these aeroelastic outputs. Uncertainty propagation studies and the parameter screening analyses showed that the variation introduced into the lift coefficient due to the horizontal tail is the most sensitive derivative relative to Young's modulus variations.

The linear analysis method employed was a perturbation analysis and thus can not be used to assess the influence of angle of attack uncertainty. This assessment was addressed with higher fidelity modeling, which utilized reduced order methods to perform the uncertainty propagation. The results of this study indicate that uncertainty in the Young's modulus associated with the structural elements of the flexible fuselage beam produce significant uncertainties in the static aeroelastic and flutter results.

The results of this study show that the flutter solution is very sensitive to the structural damping. The S^4T team showed a considerable amount of variation in their attempts to measure the modal damping. These two points lead to the undesirable conclusion that the flutter analysis is sensitive to a quantity that is difficult to accurately measure. The degree to which the flutter results are sensitive to the structural damping is dependent on, and inversely related to, the steepness of the flutter crossing.

VIII. Acknowledgments

The authors thank the S^4T project and team for their work and willingness to share the modeling, data and prior simulation results. Their thorough work in the model tuning and the deterministic baseline analysis case greatly eased the preparatory tasks for the current work.

The first author would like to thank the Istanbul Technical University Scientific Research Projects Center (BAP) for the research fund under the project titled "Computational Aeroelasticity Investigations for RTO-AVT-203 and

Aeroelastic Prediction Workshop".

References

[1]Guruswamy, G. P., "Computational-Fluid-Dynamics- and Computational-Structural-Dynamics-Based Time-Accurate Aeroelasticity of Helicopter Rotor Blades," *Journal of Aircraft*, Vol. 47, No. 3, pp. 858-863, 2010.

[2]http://overflow.larc.nasa.gov

[3]Lee-Rausch, E. M. and Batina, J. T., "Wing Flutter Computations Using an Aerodynamic Model Based on the Navier-Stokes Equations," *Journal of Aircraft*, Vol. 33, No. 6, pp. 1139-1147, 1996.

[4]Lee-Rausch, E. M. and Batina, J. T., "Wing Flutter Boundary Prediction Using Unsteady Euler Method," *Journal of Aircraft*, Vol. 2, No. 32, pp. 416-422, 1995.

[5]Giunta, A., "A Novel Sensitivity Analysis Method for High-Fidelity Multidisciplinary Optimization of Aero-Structural Systems," AIAA, 38th Aerospace Science Meeting and Exhibit, Paper 2000-0683, Reno, NV, Jan. 2000

[6]Maute, K., Nikbay, M., and Farhat, C., "Coupled Analytical Sensitivity Analysis for Aeroelastic Optimization," AIAA, 8th AIAA/USAF/NASA/ISSMO Symposium on Multidisciplinary Analysis and Optimization, Paper 2000-4825, Long Beach, CA, Sept. 2000.

[7]Maute, K., Nikbay, M., and Farhat, C., "Coupled Analytical Sensitivity Analysis and Optimization of Three-Dimensional Nonlinear Aeroelastic Systems," AIAA Journal, Vol. 39, No. 11, 2001, pp. 2051-2061. doi:10.2514/2.1227

[8]Maute, K., Nikbay, M., and Farhat, C., "Sensitivity Analysis and Design Optimization of Three-Dimensional Nonlinear Aeroelastic Systems by the Adjoint Method," International Journal for Numerical Methods in Engineering, Vol. 56, No. 6, Feb. 2003, pp. 911-933. doi:10.1002/nme.599

[9]Nikbay, M., "Coupled Sensitivity Analysis by Discrete-Analytical Direct and Adjoint Methods with Applications to Aeroelastic Optimization and Sonic Boom Minimization," Ph.D. Thesis, Univ. of Colorado at Boulder, Boulder, CO, 2002.

[10]Moller, H., and Lund, E., "Shape Sensitivity Analysis of Strongly Coupled FluidStructure Interaction Problems," AIAA, 8th AIAA/USAF/NASA/ISSMO Symposium on Multidisciplinary Analysis and Optimization, Paper 2000-4825, Long Beach, CA, Sept. 2000.

[11]Hou, G.-W., and Satyanarayana, A., "Analytical Sensitivity Analysis of a Statical Aeroelastic Wing," AIAA, 8th AIAA/USAF/NASA/ISSMO Symposium on Multidisciplinary Analysis and Optimization,Paper 2000-4825, Long Beach, CA, Sept. 2000.

[12]Gumbert, C., Hou, G.-W., and Newman, P., "Simultaneous Aerodynamic Analysis and Design Optimization (SAADO) for a 3-D Flexible Wing," AIAA, 43rd AIAA/ASME/ASCE/AHS/ASC Structures, Structural Dynamics, and Materials Conference, Paper 2002-1483, Denver, CO, April 2002.

[13]Martins, J., Alonso, J., and Reuther, J., "High-Fidelity Aero-Structural Design Optimization of a Supersonic Business Jet," AIAA, 43rd AIAA/ ASME/ASCE/AHS/ASC Structures, Structural Dynamics, and Materials Conference, Paper 2002-1483, Denver, CO, April 2002.

[14]Barcelos, M., and Maute, K., "Aeroelastic Design Optimization for Laminar and Turbulent Flows," Computer Methods in Applied Mechanics and Engineering, Vol. 197, Nos. 19-20, 2008, pp. 1813-1832. doi:10.1016/j.cma.2007.03.009

[15]Nikbay, M.,Oncu, L., and Aysan, A."Multidisciplinary Code Coupling for Analysis and Optimization of Aeroelastic Systems", AIAA Journal of Aircraft Vol. 46, No. 6, November-December 2009, DOI: 10.2514/1.41491

[16]Zhang, Z., Yang, S., Chen, P. C., "Linearized Euler Solver for Rapid Frequency-Domain Aeroelastic Analysis," *Journal of Aircraft*, Vol. 49, No. 3, pp. 922-932, 2012.

[17]NATO-STO AVT-191 Task Group Report, "Application of Sensitivity Analysis and Uncertainty Quantification to Military Vehicle Design"

[18]http://www.mscsoftware.com/product/msc-nastran

[19]http://www.zonatech.com/ZEUS.htm

[20]Perry, B., Silva, W. A., Florance, J. R., Wieseman, C. D., Pototzky, A. S., Sanetrik, M. D. et al., "Plans and Status of Wind-Tunnel Testing Employing an Aeroservoelastic Semispan Model," *48th AIAA/ASME/ASCE/AHS/ASC Structures, Structural Dynamics, and Materials Conference*, AIAA 2007-1770, Honolulu, HI, USA, 2007.

[21]Chen, P. C, Zhang, Z., Sengupta, A., and Liu, D., "Overset Euler/Boundary Layer Solver with Panel Based Aerodynamic Modeling for Aeroelastic Applications," *Journal of Aircraft*, Vol. 46, No. 6, pp. 2054-2068, 2009

[22]Wiener, N., "The homogenous chaos," *American Journal of Mathematics*, Vol. 60, pp: 897-936, 1938.

[23]Eldred, M. S., "Recent Advances in Non-Intrusive Polynomial Chaos and Stochastic Collocation Methods for Uncertainty Analysis and Designs," *50th AIAA/ASME/ASCE/AHS/ASC Structures, Structural Dynamics, and Materials Conference*, AIAA 2009-2274, Palm Springs, California, USA, 2009.

[24]Eldred, M. S. and Burkardt, J., "Comparision of Non-Intusive Polynomial Chaos and Stochastic Collocation Methods for Uncertainty Quantification," *47th AIAA Aerospace Sciences Meeting and Exhibit*, AIAA 2009-0976, Orlando, FL, USA, 2009.

[25]Witteveen, J. A. S. and Bijl, H., "Using Polynomial Chaos for Uncertainty Quantification in Problems with Nonlinearities," *47th AIAA/ASME/ASCE/AHS/ASC Structures, Structural Dynamics, and Materials Conference*, AIAA 2006-2066, Newport, Rhode Island, USA, 2006.

[26]Beran, P. and Silva, W., "Reduced Order Modeling: New Approaches to Computational Physics," *39th AIAA Aerospace Sciences Meeting and Exhibit*, AIAA 2001-0853, Reno, NV, USA, 2001.

[27]Hoetelling, H., "Simplified calculation of principal component analysis," *Psychometrica*, 1: 27-35, 1935.

[28]Bui-Thanh, T. and Willcox, K., "Model Reduction for Large Scale CFD Applications Using the Balanced Proper Orthogonal Decomposition," *17th AIAA Computational Fluid Dynamics Conference*, AIAA 2005-4617, Toronto, Canada, 2005.

[29]LeGresley, P. A. and Alonso, J., "Investigation of Non-Linear Projection for POD Based Reduced Order Models for Aerodynamics," *39th AIAA Sciences Meeting and Exhibit*, AIAA 2001-0926, Reno, NV, USA, 2001.

[30]Hall, K. C., Thomas, J. P. and Dowell, E. H., "Investigation of Non-Linear Proper Orthogonal Decomposition Technique for Transonic Unsteady Aerodynamic Flows," *AIAA Journal*, Vol. 38, No. 10, pp: 1853-1862, 2000.

[31]Thomas, J. P., Dowell, E. H. and Hall, K. C., "Three-Dimensional Transonic Aeroelasticity Using Proper Orthogonal Decomposition-Based Reduced-Order Models," *Journal of Aircraft*, Vol. 40, No. 3, pp: 544-551, 2003.

[32]Allen, M., Weickum, G. and Maute, K., "Application of Reduced Order Models for the Stochastic Design Optimization of Dynamic Systems," *10th AIAA/ISSMO Multidisciplinary Analysis and Optimization Conference*, AIAA 2004-4614, Albany, NY, USA, 2004.

[33]Chatterjee, A., "An Introduction to the Proper Orthogonal Decomposition," *Current Science-Bangalore*, Vol. 78, No. 7, pp: 808-817, 2000.

[34]Pinnau, R., "Model Reduction via Proper Orthogonal Decomposition," *Model Order Reduction: Theory, Research Aspects and Applications*, Springer, 2008.

[35]Sirovich, L., "Turbulence and the dynamics of coherent structures. IIII," *Quart. Appl. Math.*, Vol. 45, No. 3, pp: 561-590, 1987.

[36]Silva, W. A., et al. "An overview of the Semi-Span Super-Sonic Transport (S4T) wind-tunnel model program" *53rd AIAA/ASME/ASCE/AHS/ASC Structures, Structural Dynamics and Materials Conference*. Honolulu, 2012.

[37]Florance, J. R. "Lessons in the design and characterization testing of the Semi-Span Super-Sonic Transport (S4T) wind-tunnel model" *53rd AIAA/ASME/ASCE/AHS/ASC Structures, Structural Dynamics and Materials Conference*. Honolulu, 2012.

[38]Sanetrik, M. S. "Computational aeroelastic analysis of the Semi-Span Super-Sonic Transport (S4T) wind-tunnel model". *53rd AIAA/ASME/ASCE/AHS/ASC Structures, Structural Dynamics and Materials Conference*, Honolulu, 2012